Wiley Online Library
Early View publication on www.wileyonlinelibrary.com
(issue and page numbers not yet assigned;
citable using Digital Object Identifier – **DOI**)

Phys. Status Solidi B, 1600681 (2017) / **DOI** 10.1002/pssb.201600681

physica status solidi b
www.pss-b.com
basic solid state physics

Interface characterization of atomic layer deposited Al_2O_3 on m-plane GaN

Ye Jia*[,1], Joshua S. Wallace[2], Elena Echeverria[3], Joseph A. Gardella Jr.[2], and Uttam Singisetti[1]

[1] Department of Electrical Engineering, University at Buffalo, The State University of New York, Buffalo, NY 14260, USA
[2] Department of Chemistry, University at Buffalo, The State University of New York, Buffalo, NY 14260, USA
[3] Department of Physics and Astronomy, University of Nebraska, Lincoln, NE 68588, USA

Received 17 October 2016, revised 19 December 2016, accepted 5 January 2017
Published online 9 February 2017

Keywords Al_2O_3, band offset, GaN, interfaces, non-polar surfaces, X-ray photoelectron spectroscopy

* Corresponding author: e-mail yejia@buffalo.edu, Phone: +01 716 704 2864, Fax: 716-645-3656

The interfaces between dielectrics and semiconductors play a dominant role in the performance of both electronic and optoelectronic devices. In this article, we report the band offset characterization of atomic layer deposited Al_2O_3 on non-polar m-plane $(1\bar{1}00)$ GaN grown by hybrid vapor phase epitaxy using X-ray photoelectron spectroscopy (XPS). The surface band bending of GaN was investigated by employing the angle resolved XPS (ARXPS). The Fermi level pinning is found to be at ~2.4 eV above valence band maximum near the surface. The valence band offset and conduction band offset at the Al_2O_3 and m-plane GaN interface were determined to be 1.0 and 2.2 eV respectively. Electrical measurement was done by using metal–oxide–semiconductor capacitor. Capacitance–voltage hysteresis loop indicated low density of oxide traps. The frequency dependent *C–V* curves also showed a small dispersion.

1 Introduction Gallium nitride (GaN) is a widely investigated wideband gap semiconductor with a wide range of applications including high voltage power amplifiers, high speed THz devices, power switching devices, and light emitting diodes (LEDs); because of its large band gap [1], high breakdown voltage [2], and high electron mobility [3]. It also has the capability to form alloy with AlN and InN, allowing different heterostructures for various applications in electronics and optoelectronics [4–6]. In addition, the polarization fields in the wurtzite nitride system has been exploited for high mobility and polarization doping [4, 7]. However, the polarization field also reduces the doping flexibility in GaN [8]. Moreover, the polarization field reduces the efficiency of optoelectronic devices built on GaN heterostructures because of the spatial separation of electron and hole wave-functions caused by the polarization electric field [9, 10]. The polarization field has also been partially attributed to the reliability of GaN high electron mobility transistors (HEMTs) [5, 11, 12]. In order to improve the efficiency of optoelectronic devices, non-polar GaN has recently attracted a lot of attention [13–15]. The absence of the polarization field in non-polar (a- and m-plane) and semipolar GaN not only benefits LEDs and lasers [16], but also improves electronic device performance [17]. Non-polar indium nitride has been demonstrated to have an unpinned Fermi level at the surface [18]. Density functional theory (DFT) predicts that the surface Fermi level is pinned close to midgap regardless of the doping type in polar GaN [19, 20]. In contrast, the non-polar p-type GaN exhibits an unpinned Fermi level [19, 20], which can help reduce the contact resistance to p-type layers [21]. Low resistance p-contacts to GaN is useful for hetero-structure bipolar transistors [22] and p-channel GaN field effect devices in addition to LEDs and lasers [23, 24].

Understanding the interfacial properties between gate dielectric and non-polar GaN is essential for both electronic and optoelectronic devices. Atomic layer deposited (ALD) Al_2O_3 has been widely used for gate dielectrics on MOSFETs because of its large dielectric constant and band gap (~7 eV) providing small current leakage and high breakdown voltage. The band offset between high-k dielectrics and polar GaN has been intensively studied [25, 26], but there are very few reports on the interfacial properties between high-k dielectrics and non-polar m-plane GaN. In this work, we investigate the band offset of ALD-Al_2O_3 and m-plane GaN by using angle resolved X-ray photoelectron spectroscopy (XPS). The electrical properties of the interface were also characterized in MOSCAP structures.

2 Experimental

2.1 Spectroscopic characterization The m-plane bulk GaN was grown at Kyma technologies, Inc. The m-plane GaN was sliced from bulk c-plane GaN which was grown by hydride vapor phase epitaxy (HVPE). Figure 1 shows the scanning electron microscopy (SEM) and atomic force microscopy (AFM) images of the bare GaN which shows a smooth surface with a root mean square (RMS) roughness of 0.5 nm extracted from the AFM image. For band offset measurement, the Al_2O_3 films were deposited by thermal ALD at 300 °C in a Cambridge Nano Tech S100 system using trimethylaluminum (TMA) and water (H_2O).

The carrier concentration of the m-plane GaN was estimated by using Raman spectroscopy. The Raman spectrum was measured by using a Renishaw InVia Raman microscope with a 514 nm laser source. The Raman spectrum was taken in $y(z\cdot)\bar{y}$ geometry, where y is perpendicular to sample surface and z is parallel to the direction of (0001) plane. The carrier concentration could be extracted from the plasma-coupled longitudinal optical photon (LOPC) peak [27]. The intensity and the location of the LOPC is related to the plasmon frequency (ω_p) which is a function of the carrier concentration [27]:

$$\omega_p^2 = \frac{4\pi n q^2}{\varepsilon_\infty m^*}, \tag{1}$$

where the n is the carrier concentration, ε_∞ is the dielectric constant at high frequency and the m^* is the effective carrier mass.

The XPS spectra were acquired by using a Physical Electronic PHI VersaProbe 5000 equipped with a hemispherical energy analyzer. A monochromic Al Kα X-ray source (1486.6 eV) was operated at 25.3 W and 15 kV. High resolution spectra were acquired by operating the analyzer at a pass energy of 11.75 eV and were used to characterize the valence band offset (VBO). The energy resolution was 0.025 eV. The acquisitions were performed under ultrahigh vacuum conditions (operating pressure $< 4 \times 10^{-6}$ Pa, background pressure $< 1 \times 10^{-6}$ Pa). The effect of surface charging on the acquired signal was reduced by utilizing dual charge neutralization in the XPS measurement. Electron and Ar ion neutralization was used.

The binding energies were aligned by setting the CH_x peak in the C 1*s* envelope at 284.8 eV to correct for the charging effects [28] within an error of ±0.1 eV. Angle resolved measurements for valence band at same condition were performed at take-off angles ranging from 15° to 75° at 15° increments. With the increasing take-off angle, the sampling depth of XPS became deeper inside substrate [29].

The XPS spectra were curve fitted with Voigt band function after Shirley background subtraction with following limits: binding energy ±0.2 eV, FWHM ±0.4 eV, and 92% Gauss. The valence band offset (VBO) was extracted by the method given by Kraut et al. [30]:

$$\begin{aligned}\Delta E_v = &\left(E^{Al2p}_{Al_2O_3/GaN} - E^{Ga2p_{3/2}}_{Al_2O_3/GaN}\right)\\ &+ \left(E^{Ga2p_{3/2}}_{GaN} - E^{VBM}_{GaN}\right)\\ &- \left(E^{Al2p}_{Al_2O_3} - E^{VBM}_{Al_2O_3}\right),\end{aligned} \tag{2}$$

where the superscripts represent XPS core level peaks and subscripts represent the samples. Three different samples were analyzed: 50 nm Al_2O_3 on GaN, bare GaN, and ~3 nm Al_2O_3 on GaN. The terms $E^{Ga2p_{3/2}}_{GaN} - E^{VBM}_{GaN}$ and $E^{Al2p}_{Al_2O_3} - E^{VBM}_{Al_2O_3}$ were calculated through the XPS spectra of the bare GaN and the GaN with 50 nm Al_2O_3. The term $E^{Al2p}_{Al_2O_3/GaN} - E^{Ga2p_{3/2}}_{Al_2O_3/GaN}$ was obtained from the XPS spectra of the 3 nm Al_2O_3/GaN heterojunction. The conduction band offset (CBO) can be found by

$$\Delta E_c = \Delta E_g - \Delta E_v, \tag{3}$$

where ΔE_g is the band gap difference between Al_2O_3 and GaN and ΔE_v is the VBO. The bandgap of an insulator can

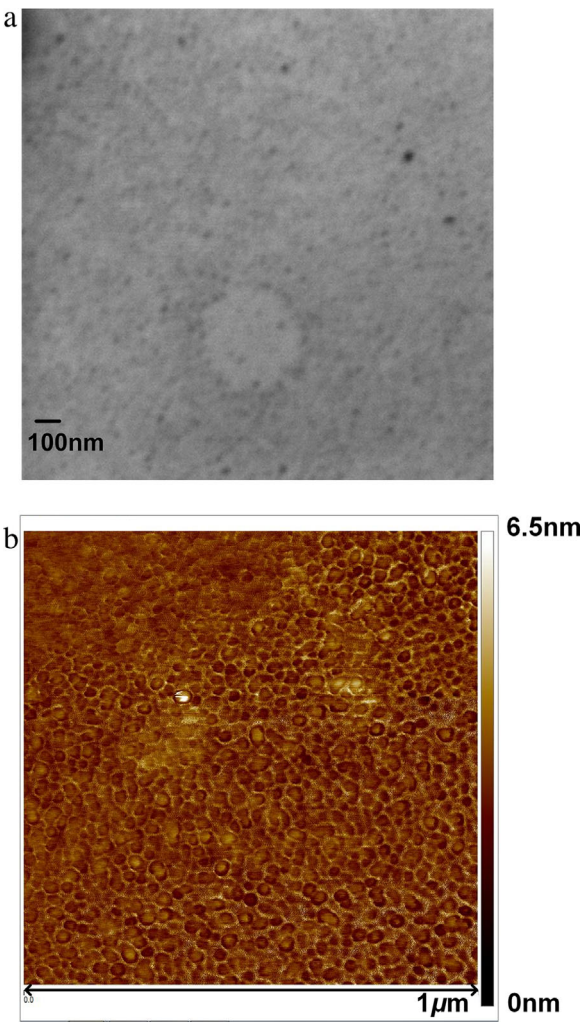

Figure 1 (a) SEM and (b) AFM image of bare GaN. The RMS roughness was extracted to be 0.5 nm.

be determined from the threshold energy of its loss energy spectrum [31].

2.2 Electrical characterization The electrical properties of the interface were measured using metal–oxide–semiconductor capacitor (MOSCAP). The main challenge of fabricating a MOSCAP is the formation of ohmic contact between metal and GaN surface due to the surface Fermi level pinning. It has been reported that the ohmic contact could be achieved by employing reactive ion etching and thermal treatment [32]. The wafer was firstly subjected to 2 min buffered-HF cleaning to remove any oxide layer on top of GaN. Next, the wafer was exposed to an inductively coupled plasma reactive ion etch (ICP-RIE). The power of ICP and RIE was set to be 300 W and 200 W, respectively. A gas combination of BCl_3 and Cl_2 was used. The bottom contacts (S/D contacts) were patterned using electron beam lithography (EBL), followed by the deposition of a metal layer that consists of Ti/Al/Ni/Au in electron beam evaporator. Following a lift-off process, the wafer was annealed at 950 °C in a rapid thermal annealing (RTA) system. Next, the Al_2O_3 was deposited in ALD system at 300 °C. A top gate contact (Ni/Au) was also defined by EBL and lift-off process. Since the S/D contacts were covered by the dielectric, an additional S/D contact opening was required, utilizing an alumina etchant.

Prior to the capacitance–voltage measurement, the leakage current was measured on the MOSCAPs using Agilent 4155B semiconductor parameter analyser. With a small leakage current, the *C–V* measurements were performed using Agilent 4294A impedance analyzer with 42941A impedance probe. The *C–V* hysteresis loop was measured at a frequency of 1 MHz with an oscillation level of 20 mV. The frequency dependent *C–V* curves were obtained at a frequency range of 10 kHz to 1 MHz.

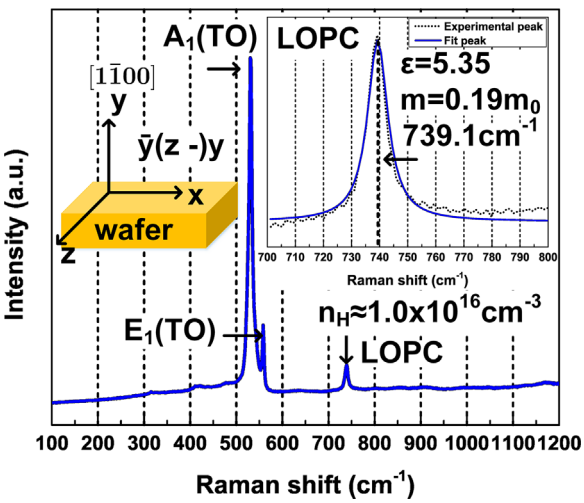

Figure 2 Raman spectroscopy of the GaN. The inset shows the experimental and fitted LOPC peak. A carrier concentration of $1.0 \times 10^{16}\,\mathrm{cm}^{-3}$ was determined.

3 Results and discussion

3.1 Spectroscopic characterization Figure 2 shows the Raman spectroscopy spectrum taken in $y(z\cdot)\bar{y}$ geometry. The inset of Fig. 2 shows the LOPC peak [27]. We observed A_1 (TO) [27, 33] at 530.5 cm^{-1}, E_1 (TO) [27] at 558.2 cm^{-1}, and LOPC peak [27] at 739.1 cm^{-1}. The observation of E_1 (TO), which is forbidden in this geometry in non-polar GaN [33], is attributed to the polarity mixture due to the miscut in the slicing process. Assuming a high frequency dielectric constant of 5.35 and effective electron mass of $0.19m_0$, where m_0 is the electron mass, the fitting of the LOPC peak [27] gave a carrier concentration of $\sim 1.0 \times 10^{16}\mathrm{cm}^{-3}$ which is in good agreement with the value obtained from Hall measurement ($n = 1.1 \times 10^{16}\mathrm{cm}^{-3}$).

Figure 3a shows the XPS spectrum of the as-received GaN. We observed a very strong Ga–O peak at 1,120.0 eV compared to the Ga–N peak at 1,118.9 eV, suggesting a thick native oxide layer. It has been reported that the hydrofluoric acid (HF) could

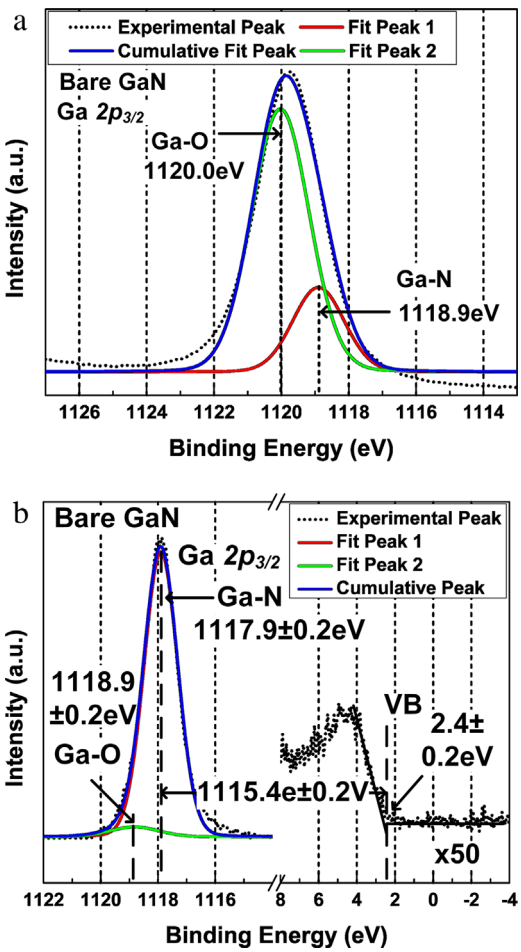

Figure 3 (a) XPS spectrum of the as-received GaN. The Ga–O peak at 1,120.0 eV was much stronger than the Ga–N peak at 1,118.9 eV, suggesting very thick native oxide layer on top of GaN. (b) Ga 2*p*3/2 peak and valence band maximum acquired from bare GaN after etching of the native oxide in HF. The native oxide was effectively removed after HF as a very small Ga–O peak was observed from Ga 2*p*3/2 peak as shown in (b).

remove native oxide on GaN effectively [34]. Therefore, the surface oxides were removed by etching for 2 min in hydrofluoric acid (HF) which gave sharp Ga–N peaks with minimal Ga–O peak as shown in Fig. 3b. The Ga $2p_{3/2}$ spectrum from bare GaN in Fig. 3b showed a small peak at 1,118.9 eV corresponding to Ga–O bond in additional to the Ga–N peak at 1117.9 eV, suggesting a very thin native oxide layer remaining on top of GaN after the HF cleaning. The angle-resolved XPS spectra of the bare GaN after HF etching were acquired to investigate the Fermi level pinning near the surface.

Figure 4 shows the valence band spectra at different take-off angles acquired from the bare GaN after HF cleaning. The valence band maxima (VBM) were found by the linear extrapolation of the leading edge of the XPS spectra [31]. At 30°, 45°, 60°, and 75°, the Fermi level near the surface was at 2.3–2.5 eV above the VBM. We were unable to extract the VBM at 15° due to the very weak signal. The position of surface Fermi level with respect to the VBM was in accordance with the value predicted by DFT (0.7 eV below conduction band minimum) [19, 20]. The non-polar m-plane GaN exhibited similar surface Fermi level pinning compared to polar GaN [35, 36].

Figure 5a and b show the XPS spectra acquired from the GaN with 50 nm Al_2O_3 and 3 nm Al_2O_3/GaN heterojunction at a take-off angle of 45°, respectively. From XPS spectra at the take-off angle of 45°, the $E_{GaN}^{Ga2p_{3/2}} - E_{GaN}^{VBM}$ and $E_{Al_2O_3}^{Al2p} - E_{Al_2O_3}^{VBM}$ were calculated to be 1,115.4 and 71.2 eV. The peak position of Ga $2p_{3/2}$ with respect to the VBM was in good agreement with reported values (1115.49−1116.47 eV) [37–39]. The energy difference between Al 2p and VBM of Al_2O_3 was comparable to the reported thermal ALD-Al_2O_3 (70.74−71.75 eV) [40–45], plasma enhanced ALD-Al_2O_3 (70.5 eV) [46] and (0001) sapphire (70.84−70.85 eV) [47, 48]. The $E_{Al_2O_3/GaN}^{Al2p} - E_{Al_2O_3/GaN}^{Ga2p_{3/2}}$ was found to be −1043.2 eV, giving a valence band offset (ΔE_v) of

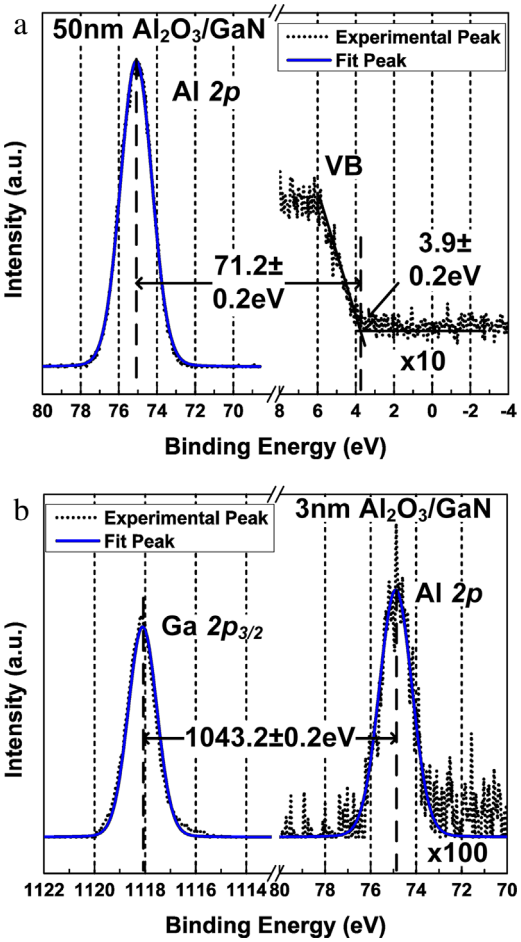

Figure 5 XPS spectra used to calculate the valence band offset. (a) Al 2*p* peak and valence band maximum acquired from 50 nm Al_2O_3/GaN. (b) Ga $2p_{3/2}$ peak and Al 2*p* peak obtained from ~3 nm Al_2O_3/GaN heterostructure. The valence band offset was calculated to be ~1.0 eV.

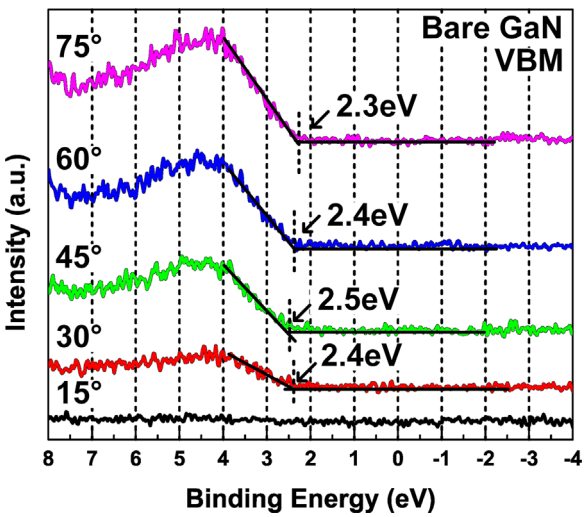

Figure 4 The valence band XPS spectra at different take-off angles. The VBM was extracted to be 2.3–2.5 eV below Fermi level from 30° to 75°.

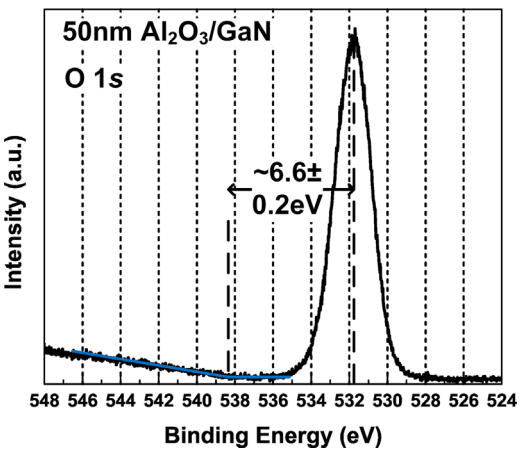

Figure 6 O 1*s* peaks obtained from 50 nm Al_2O_3/GaN to determine the bandgap of Al_2O_3. The bandgap of Al_2O_3 was found to be 6.6 eV.

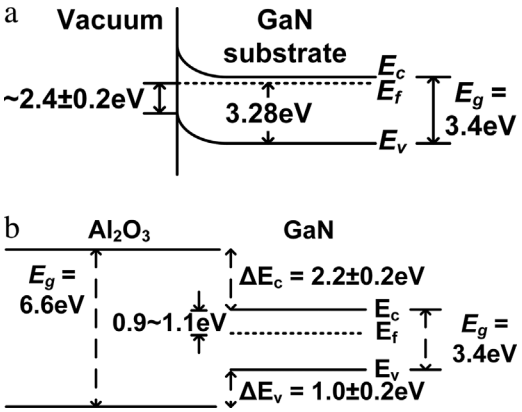

Figure 7 (a) Band diagram of the bare GaN. (b) Band diagram of the Al_2O_3/GaN heterostructure.

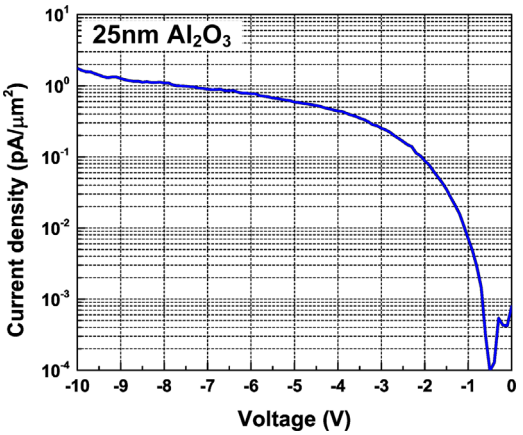

Figure 9 Leakage current. A small leakage current was obtained, revealing a good quality of dielectric layer.

1.0 eV. Figure 6 shows the core level of O 1*s* obtained from the 50 nm Al_2O_3/GaN sample. The bandgap of Al_2O_3 was found to be 6.6 eV, which agreed with the values reported in literature [40, 46]. Considering the bandgap of GaN as 3.4 eV [1], a CBO of 2.2 eV was obtained. The VBO values obtained here are comparable to the recently reported VBO value of 0.7–0.9 eV [26] between thermal ALD-Al_2O_3 and c-plane GaN. While, the VBO values are higher (VBO: 1.7–1.8 eV [49]) in plasma enhanced ALD-Al_2O_3 and Ga-polar GaN compared to the values reported here. The extracted larger CBO between thermal ALD-Al_2O_3 and m-plane GaN is beneficial for electronic applications. Recently, a VBO of 0.63 eV between a-plane AlN and a-plane GaN has been reported [50]. Assuming a band gap of 6.2 eV [51] for AlN, a CBO of 2.17 eV was obtained which was comparable to ALD-Al_2O_3 and m-plane GaN. With a post deposition annealing, the valence band offset between thermal ALD/CVD-Al_2O_3 and polar GaN could be reduced [25, 52]. Figure 7a and b shows the simulated band structure of the bare GaN and the heterostructure at Al_2O_3/GaN interface respectively with measured band parameters. Compared to the upward band bending of 0.345 eV on Ga-face GaN with a Si doping concentration of $4 \times 10^{17} cm^{-3}$ reported in Ref. [29], our m-plane GaN surface exhibited a large upward band bending of 0.88 eV.

Due to the extraction of the valence band, there was an error of 0.2 eV in determination of the energy difference between core level and VBM. Although dual neutralization was used to reduce the charging effects, the differential surface charging between GaN and Al_2O_3 can introduce error in extracting binding energies of core level and calculating the band offsets, especially in a short scanning period [53].

3.2 Electrical characterization The electrical characterization was done by utilizing MOSCAP as mentioned above. All the measurements were done in low-light environment to avoid light generated electron-hole pairs. In order to reasonably characterize MOSCAP, verification of the ohmic contact was carried out by measuring the *I–V* curve on two adjacent S/D contacts. Figure 8 shows the post annealing *I–V* curve, indicating ohmic contact.

The leakage current of MOSCAP was then measured, shown in Fig. 9. It was found that the leakage current was

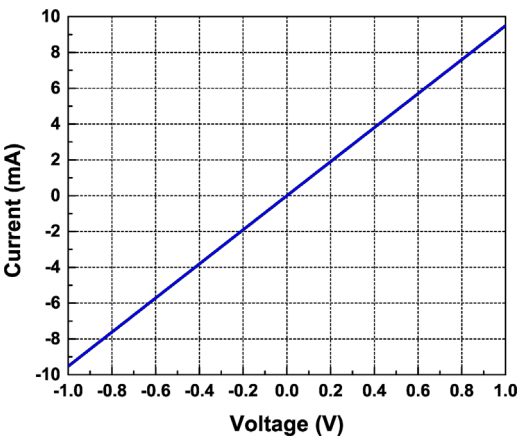

Figure 8 *I–V* curves of the two adjacent S/D contacts after annealing. The linear *I–V* indicates an ohmic contact.

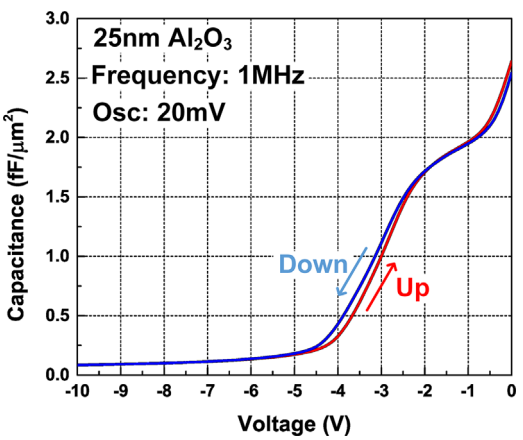

Figure 10 *C–V* hysteresis loop. A small dispersion was observed between the two directions indicating low density of oxide traps.

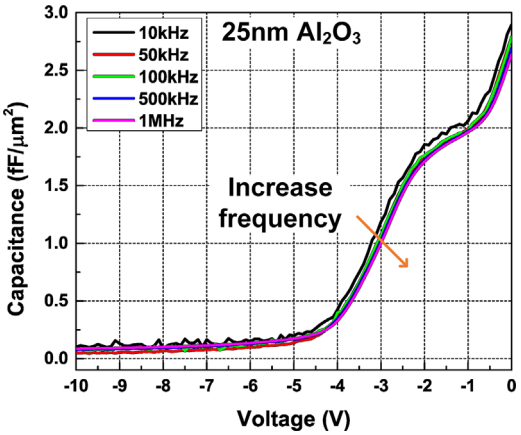

Figure 11 Frequency dependent *C–V* curves. A small dispersion was observed.

small. At −10V, the leakage current was around 1 pA μm^{-2}. With the small leakage current, the capacitance–voltage was characterized. Figure 10 shows the *C–V* hysteresis loop at frequency of 1 MHz. This measurement was done by sweeping gate voltage up and down. The dispersion of the *C–V* curves reflects oxide traps. However, in our study, the dispersion was very small, indicating a low density of oxide traps [54]. Figure 11 shows the frequency dependent *C–V* curves. The *C–V* curves were obtained at 10 kHz, 50 kHz, 100 kHz, 500 kHz, and 1 MHz. With increasing frequency, the *C–V* curve shifted to positive voltage. Although a dispersion was observed, it was small so that the density of interface trap could be low. Further advanced temperature dependent capacitance and conductance voltage characterization are needed to quantitatively extract the interface trap density across the bandgap.

4 Summary We investigated the band offset between ALD-Al_2O_3 and m-plane GaN by XPS. The valence band offset and conduction band offset were determined to be 1.0 and 2.2 eV, respectively. A large conduction band offset is desired to reduce the current leakage though the MOS junction. Angle resolved XPS of the valence band shows that the Fermi level is pinned at 1.0 eV below the conduction band edge which was in good agreement with DFT calculations and also with Fermi level pinning in polar n-GaN reported in literatures. *I–V* curve of MOSCAP exhibited a small leakage current. *C–V* hysteresis loop revealed a good quality of the interface and the small frequency dispersion indicated a potentially low density of interface trap (D_{it}).

Acknowledgements This work was supported by ONR grant (N000141310214) monitored by Dr. Paul A. Maki and by the Innovative Micro-Programs Accelerating Collaboration in Themes (IMPACT) program funded by the Office of Vice President of Research and Economic Development at the University at Buffalo. A portion of this work was performed in the UB shared instrumentation facility.

References

[1] J. F. Muth, J. H. Lee, I. K. Shmagi, R. M. Kolbas, H. C. Casey, B. P. Keller, U. K. Mishra, and S. P. DenBaars, Appl. Phys. Lett. **71**, 2572 (1997).
[2] Y. F. Wu, B. P. Keller, S. Keller, D. Kapolnek, P. Kozodoy, S. P. Denbaars, and U. K. Mishra, Appl. Phys. Lett. **69**, 1438 (1996).
[3] D. C. Look, D. C. Reynolds, J. W. Hemsky, J. R. Sizelove, R. L. Jones, and R. J. Molnar, Phys. Rev. Lett. **79**, 2273 (1997).
[4] B. Reuters, A. Wille, N. Ketteniss, H. Hahn, B. Holländer, M. Heuken, H. Kalisch, and A. Vescan, J. Electron. Mater. **42**, 826 (2013).
[5] T. Oka and T. Nozawa, IEEE Electron. Device Lett. **29**, 668 (2008).
[6] S. J. Chang, C. H. Kuo, Y. K. Su, L. W. Wu, J. K. Sheu, T. C. Wen, W. C. Lai, J. F. Chen, and J. M. Tsai, IEEE J. Sel. Top. Quantum Electron. **8**, 744 (2002).
[7] Y. Fang, Z. Feng, J. Yin, X. Zhou, Y. Wang, G. Gu, X. Song, Y. Lv, C. Li, and S. Cai, IEEE Trans. Electron Devices **61**, 4084 (2014).
[8] T. Paskova, Nitrides with Nonpolar Surfaces: Growth, Properties, and Devices (Wiley-VCH, Weinheim, 2008), p.3.
[9] S. -H. Park, D. Ahn, and S. -L. Chuang, J. Quantum Electron. **43**, 1175 (2007).
[10] D. Hanser, M. Tutor, E. Preble, M. Williams, X. Xu, D. Tsvetkov, and L. Liu, J. Cryst. Growth **305**, 372 (2007).
[11] O. Ambacher, J. Smart, J. R. Shealy, N. G. Weimann, K. Chu, M. Murphy, W. J. Schaff, and L. F. Eastman, J. Appl. Phys. **85**, 3222 (1999).
[12] E .T. Yu, X. Z. Dang, P. M. Asbeck, S. S. Lau, and G. J. Sullivan, J. Vac. Sci. Technol. B **17**, 1742 (1999).
[13] A. Chakraborty, B. A. Haskell, S. Keller, J. S. Speck, S. P. Denbaars, S. Nakamura, and U. K. Mishra, Jpn. J. Appl. Phys. **44**, L173, (2005).
[14] M. C. Schmidt, K. -C. Kim, R. M. Farrell, D. F. Feezell, D. A. Cohen, M. Saito, K. Fujito, J. S. Speck, S. P. DenBaars, and S. Nakamura, Jpn. J. Appl. Phys. **46**, L190, (2007).
[15] R. M. Farrell, D. F. Feezell, M. C. Schmidt, D. A. Haeger, K. M. Kelchner, K. Iso, H. Yamada, M. Saito, K. Fujito, D. A. Cohen, J. S. Speck, S. P. DenBaars, and S. Nakamura, Jpn. J. Appl. Phys. **46**, L761 (2007).
[16] T. Paskova, Nitrides with Nonpolar Surfaces: Growth, Properties, and Devices (Wiley-VCH, Weinheim, 2008) p.23.
[17] M. Kuroda, H. Ishida, T. Ueda, and T. Tanaka, J. Appl. Phys. **102**, 093703 (2007).
[18] Y. Jia, J. S. Wallace, Y. Qin, J. A. Gardella, A. M. Dabiran, and U. Singisetti, J. Electron. Mater. **45**, 2013 (2015).
[19] C. G. Van de Walle and D. Segev, J. Appl. Phys. **101**, 081704 (2007).
[20] D. Segev and C. G. Van de Walle, Europhys. Lett. **76**, 305 (2006).
[21] M. McLaurin, T. E. Mates, F. Wu, and J. S. Speck, J. Appl. Phys. **100**, 063707 (2006).
[22] L. S. McCarthy, P. Kozodoy, M. J. W. Rodwell, S. P. DenBarrs, and U. K. Mishra, IEEE Electron Device Lett. **20**, 277 (1999).
[23] S. Nakamura, Diam. Relat. Mater. **5**, 496 (1996).
[24] J. -O. Song, D. -S. Leem, S. -H. Kim, J. S. Kwak, O. H. Nam, Y. Park, and T. -Y. Seong, Solid-State Electron. **48**, 1597 (2004).

[25] M. R. Coan, J. H. Woo, D. Johnson, I. R. Gatabi, and H. R. Harris, J. Appl. Phys. **112**, 024508 (2012).
[26] T. L. Duan, J. S. Pan, and D. S. Ang, Appl. Phys. Lett. **102**, 201604 (2013).
[27] B. Ma, D. Jinno, H. Miyake, K. Hiramatsu, and H. Harima, Appl. Phys. Lett. **100**, 011909 (2012).
[28] C.-F. Shih, N.-C. Chen, P.-H. Chang, and K.-S. Liu, Jpn. J. Appl. Phys. **44**, 7892 (2005).
[29] T. L. Duan, J. S. Pan, and D. S. Ang, ECS J. Solid State Sci. Technol. **5**, P514 (2016).
[30] E. A. Kraut, R. W. Grant, J. R. Waldrop, and S. P. Kowalczyk, Phys. Rev. Lett. **44**, 1620 (1980).
[31] S. A. Chambers, T. Droubay, T. C. Kaspar, and M. Gutowski, J. Vac. Sci. Technol. B **22**, 2205 (2004).
[32] Z. Fan, S. N. Mohammad, W. Kim, O. Z. R. Aktas, A. E. Botchkarev, and H. Morkoç, Appl. Phys. Lett. **68**, 1672 (1996).
[33] K. Fujito, K. Kiyomi, T. Mochizuki, H. Oota, H. Namita, S. Nagao, and I. Fujimura, Phys. Status Solidi A **205**, 1056 (2008).
[34] L. L. Smith, S. W. King, R. J. Nemanich, and R. F. Davis, J. Electron. Mater. **25**, 805 (1996).
[35] P. Lorenz, T. Haensel, R. Gutt, R. J. Koch, J. A. Schaefer, and S. Krischok, Phys. Status Solidi B **247**, 1658 (2010).
[36] S.-C. Lin, C.-T. Kuo, X. Liu, L.-Y. Liang, C.-H. Cheng, C.-H. Lin, S.-J. Tang, L.-Y. Chang, C.-H. Chen, and S. Gwo, Appl. Phys. Express **5**, 031003 (2012).
[37] G. Martin, A. Botchkarev, A. Rockett, and H. Morkoç, Appl. Phys. Lett. **68**, 2541 (1996).
[38] P. D. C. King, T. D. Veal, C. E. Kendrick, L. R. Bailey, S. M. Durbin, and C. F. McConville, Phys. Rev. B **78**, 033308 (2008).
[39] M. Kumar, M. K. Rajpalke, B. Roul, T. N. Bhat, A. T. Kalghatgi, and S. B. Krupanidhi, Phys. Status Solidi B **249**, 58, (2012).
[40] M. L. Huang, Y. C. Chang, C. H. Chang, T. D. Lin, J. Kwo, T. B. Wu, and M. Hong, Appl. Phys. Lett. **89**, 012903 (2006).
[41] J. W. Liu, M. Y. Liao, M. Imura, and Y. Koide, Appl. Phys. Lett. **101**, 252108 (2012).
[42] X. Wang, J. Xiang, W. Wang, J. Zhang, K. Han, H. Yang, X. Ma, C. Zhao, D. Chen, and T. Ye, Appl. Phys. Lett. **102**, 031605 (2013).
[43] A. Rifai, S. Maikap, and Y. Nakamura, J. Vac. Sci. Technol. B **33**, 051812 (2015).
[44] A. Maréchal, M. Aoukar, C. Vallée, C. Rivière, D. Eon, J. Pernot, and E. Gheeraert, Appl. Phys. Lett. **107**, 141601 (2015).
[45] J. W. Liu, M. Imura, and Y. Koide, J. Appl. Phys. **120**, 124504 (2016).
[46] T. Kamimura, K. Sasaki, M. Hoi Wong, D. Krishnamurthy, A. Kuramata, T. Masui, S. Yamakoshi, and M. Higashiwaki, Appl. Phys. Lett. **104**, 192104 (2014).
[47] J. Distefano, Y. -C. Lin, J. Robinson, N. R. Glavin, A. A. Voevodin, J. Brockman, M. Kuhn, B. French, and S. W. King, J. Electron. Mater. **48**, 983 (2016).
[48] J. Tao, J. W. Chai, Z. Zhang, J. S. Pan, and S. J. Wang, Appl. Phys. Lett. **104**, 232110 (2014).
[49] J. Yang, B. S. Eller, C. Zhu, C. England, and R. J. Nemanich, J. Appl. Phys. **112**, 053710 (2012).
[50] H. Li, X. Liu, L. Sang, J. Wang, D. Jin, H. Zhang, S. Yang, S. Liu, Y. Hao, Q. Zhu, and Z. Wang, Phys. Status Solidi B **251**, 788 (2014).
[51] J. Wu and W. Walukiewicz, Superlattices Microstruct. **34**, 63 (2003).
[52] S. Toyoda, T. Shinohara, H. Kumigashira, M. Oshima, and Y. Kato, Appl. Phys. Lett. **101**, 231607 (2012).
[53] E. Bersch, M. Di, S. Consiglio, R. D. Clark, G. J. Leusink, and A. C. Diebold, J. Appl. Phys. **107**, 043702 (2010).
[54] A. Winzer, N. Szabó, A. Wachowiak, P. M. Jordan, J. Heitmann, and T. Mikolajick, J. Vac. Sci. Technol. B **33**, 01A106 (2015).